Electrochemical Impedance Studies of Co-Based Nanomaterials for Hydrogen Evolution Reaction

J.V. Medina, E. M. Arce, J. G. López

Instituto Politécnico Nacional. ESIQIE. Departamento de Ingeniería en Metalurgia y Materiales, México, D.F.

ABSTRACT

The electrocatalytic activity for hydrogen evolution reaction (HER) of cobalt based nanomaterials synthesized by high energy mechanical milling was studied to use in PEM electrolyzers. X-ray diffraction, scanning electron microscopy and transmission electron microscopy were used to characterize the synthesized powders. Their composition was established by means of energy dispersive spectroscopy, showing the presence of iron which was caused by the wear of grinding medium. Analysis SEM and TEM showed the formation of agglomerates of 1-5 microns, constituted by particles close to 20 nanometers. The electrocatalytic activity of the materials $Co_{80}Ru_{20}$ and $Co_{80}Ru0_{15}Pt_5$ in acid medium was evaluated in 0.5 M H_2SO_4 at 25 °C using linear polarization technique and electrochemical impedance spectroscopy (EIS). From polarization curves was possible to determinate the mechanism of HER. Nyquist diagrams were obtained in a frequency range from 100 kHz to 10 mHz at selected overpotentials in order to avoid the formation of bubbles on the surface of electrode. These diagrams showed the presence of two semicircles, the diameter of the first one, at high frequency, remained constant at all overpotentials, while the diameter of the second one, at low frequency, decreased when overpotential increased. Electrical equivalent circuit 2-CPE was used for the purpose of explaining the electrochemical response. The kinetic parameters for HER obtained from analysis of polarization and impedance data showed that both materials exhibit good performance as electrocatalysts toward to HER. The material with the best performance was $Co_{80}Ru0_{15}Pt_{5.}$

Keywords: Impedance; linear polarization; hydrogen evolution reaction

1. Introduction

The carbon dioxide emissions from human activities and the expected depletion of oil reserves are the subject of a global debate about energetic sustainability and climatic stability, accelerating global initiatives to develop new renewable energy systems [1]. In spite of the energy sources of the future there will always be a need for convenient, clean, safe, efficient and versatile energy carriers or forms of energy that can be delivered to the end user. One of these energy carriers is electricity, already being used worldwide. Electricity is a convenient form of energy, produced from various sources and transported over large distances. It is clean, although its production from fossil fuels is not. Hydrogen is another clean, efficient and versatile energy carrier, supplemented electricity very well. Together these two carriers may satisfy all the energy needs and form an energy system that is permanent and independent of energy sources [3-4]. However, hydrogen is not a primary energy source, in nature cannot be found it in elemental or molecular form, only taking part of different compounds, water being the most abundant source. H_2 can be produced from a wide range of material, including fossil fuels, biomass and water electrolysis [5].

Water electrolysis is relatively efficient (>70%), but because it needs electricity, hydrogen produced by water-electrolysis is expensive, and this is due to the laws of thermodynamics, inasmuch the energy required to separate the H_2 and O_2 from water is higher than the energy which can be released by hydrogen utilization [6]. Hydrogen can be produced efficiently using electricity from renewable energy sources such as solar and wind [7]. In conventional PEM water electrolyzers, precious metals are used as electrocatalysts, implying one of the most important issues about the choice of the electrodes materials for hydrogen and oxygen evolution. The ability of a given metal to catalyze the HER is usually measured by the exchange current density. Three properties play an important role in selecting catalytically active materials for hydrogen evolution: (a) an actual intrinsic electrocatalytic effect of the material, (b) a large active surface area per unit volume ratio, both of which are directly related to the overpotential used to operate the electrolyzer at significant current densities, and (c) catalyst stability [8]. Platinum was found to be an electrode material on the top of which hydrogen evolves with the minimum overpotential [9]. Unfortunately, due to the high price and limited resources, the application of Pt in the future will be limited [10]. One of the main challenges in PEM technologies is to reduce noble metals contents or completely replace them and to maintain the same level of efficiency [11]. Alternatively non-precious metals, such as Ni, Co and their allows have been studied for HER, but the activity of these systems in electrolyzers PEM was poor due to instability en acid medium [12].

In this work, cobalt based nanostructured materials were prepared by mechanical alloying and were characterized by scanning electron microscopy; crystallite size was obtained by means X-ray diffraction using Sherrer and Williamson-Hall methodologies. The catalytic properties toward HER were described by Tafel linear and Electrochemical Impedance Spectroscopy (EIS).

2. Experimental

2.1. Electrode preparation

Preparation of the catalytic powders was performed by the mechanical alloying technique, two different systems were tested $Co_{80}Ru_{20}$ and $Co_{80}Ru_{15}Pt_5$, Co (Sigma-Aldrich 325 mesh powder), Ru (Sigma-Aldrich 200 mesh powder) and Pt (Sigma-Aldrich 1 µm) were introduced in a high energy ball mill Spex 8000 during 40 h using a stainless steel vial and balls with a ball to powder ratio of 4:1. Their chemical composition, in *wt.%*, was tested by Energy Dispersive Spectroscopy. The carbon paste used as working electrode was prepared as follows: 0.1 g of metallic phase and 0.4 g of graphite were mixed with 0.25 mL of silicone oil. The carbon paste obtained was packed into a polypropylene holder to control the exposed surface. Electrical contact to the paste was established via a thin copper rod passed through the polypropylene holder.

2.2. Electrochemical setup

A conventional glass cell was used with a separated compartment for the reference electrode. The reference electrode was a mercury-potassium sulfate electrode Hg/K_2SO_4 (E = 0.64 V/NHE). All potentials are referred to NHE. A graphite bar was used as counter electrode. All electrochemical measurements: the *dc* polarization and the electrochemical impedance spectroscopy (EIS) were carried out in aqueous acid 0.5 M H_2SO_4, bubbled with ultra-high purity nitrogen to remove the present oxygen. The flux of nitrogen was maintained above the electrolyte surface during the measurements. The temperature at which the measurements were performed was at 25 °C, controlled by means an isothermal bath. Polarization measurements of hydrogen evolution were carried out by first stabilization at open-circuit potential (OCP), then a linear polarization measurement was conducted starting from OCP to negative direction, at a scan rate of 5 mV s^{-1}. Electrochemical impedance spectroscopy measurements were performed at selected overpotentials of 0 V, -0.010 V, -0.025 V y -0.035 V.

2.3. Apparatus and methods

A D5000 SIEMENS X-ray diffractometer using Mo Kα radiation and operating at 35 kV and 25 mA was utilized for the structural and phase analysis of the obtained powders. The XRD patterns were recorded in a 2θ range from 10 to 70° at a step time of 0.5° min^{-1}. The particles and their surface morphologies were examined using Transmission Electron Microscope JEOL 2000-FXII and a field emission scanning electron microscope JEOL JSM-6701F equipped with an energy dispersive spectrometer. Electrochemical measurements were performed using a Potentiostat/Galvanostat Autolab-30 system connected to a personal computer.

3. Results and discussion

3.1. XRD analysis

The present phases in the studied powders were identified by using XRD analysis. XRD spectra are shown in fig. 1.

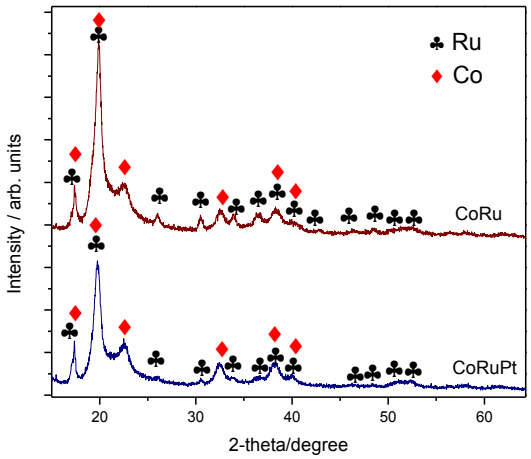

Fig. 1. XRD patterns of $Co_{80}Ru_{20}$ and $Co_{80}Ru0_{15}Pt_5$ powders after 40h milling time.

Co and Ru both presented a HCP crystalline structure before they were submitted to milling, but the characteristic peaks for Co after milling do not correspond to this structure, so there was a change phase, corresponding to FCC structure, in the other hand, the characteristic peaks for Ru were the same, XRD spectra do not show evidence of

formation of intermetallic compounds, because new peaks do not appear, although there are overlapping in certain characteristic peaks. The presence of platinum was not detected; this could be attributed to its low percentage or its small crystallite size.

It was estimated crystallite size by means Sherrer [13] and Williamson-Hall [14] methodologies, table 1 lists the values obtained. Sherrer methodology assume that microdeformations in the crystal lattice are negligible, unfortunately in the preparation of electrocatalysts by mechanical milling technique the presence of microdeformations in the crystal lattices of the materials are inevitable, leading the crystallite size estimated using Sherrer to an erroneous result. Considering this situation, other methodologies are needed to estimate the crystallite size, where the broadening of the peak due to microstrains is considered. Williamson-Hall methodology considers this situation and it is possible to employ the different kind of profile of diffraction peaks (Gaussian, Lorentzian and Pseudo-Voigth). The calculated values from these methodologies are displayed in the table 1, the values from Scherrer methodology are completely different to values from Williamson-Hall methodology this is due to the mentioned above, on the other hand, values from Gaussian profile are different from other profiles, results from Lorentzian profile are so similar to Pseudo-Voigth results, inasmuch as Pseudo-Voigth profile let combine Gaussian and Lorentzian profiles it can be taken this value like the most reliable.

Table 1. Crystallite sizes calculated from XDR data.

	Cristallyte size (nm)			
Sample	**Williamson-Hall**			**Sherrer**
	Profile			
	Gaussian	Lorentzian	Pseudo-Voigth	
$Co_{80}Ru_{20}$	15.71	21.42	21.74	14.7
$Co_{80}Ru_{15}Pt_5$	18.78	24.99	24.68	17.55

3.2. SEM and TEM analysis

SEM and TEM analysis was performed to observe the particle size and the morphology of the prepared electrocatalyst, fig. 2. In both electrocatalysts agglomerates from 1 to 5 microns in size were formed, conformed by particles lower close to 20 nm, this confirms the results obtained from XDR analysis. From fig. 2 a, corresponding to the micrograph of $Co_{80}Ru_{20}$ system, it can be seen that the particles are slightly smaller than particles of system $Co_{80}Ru_{15}Pt_5$, fig. 2b.

The composition and content of CoRu and CoRuPt were established by means EDS analysis. Fig. 2 also shows EDS spectra of a) $Co_{80}Ru_{20}$ and b) $Co_{80}Ru_{15}Pt_5$ and it can be observed the presence of the characteristic lines of iron, stemming from the grinding media wear, iron modifies the nominal composition, so the weight ratio of Co, Ru and Fe is 73:20:7 for Co-Ru, and for Co-Ru-Pt the weight ratio of Co, Ru, Pt and Fe is 78:15:5:2.

a)

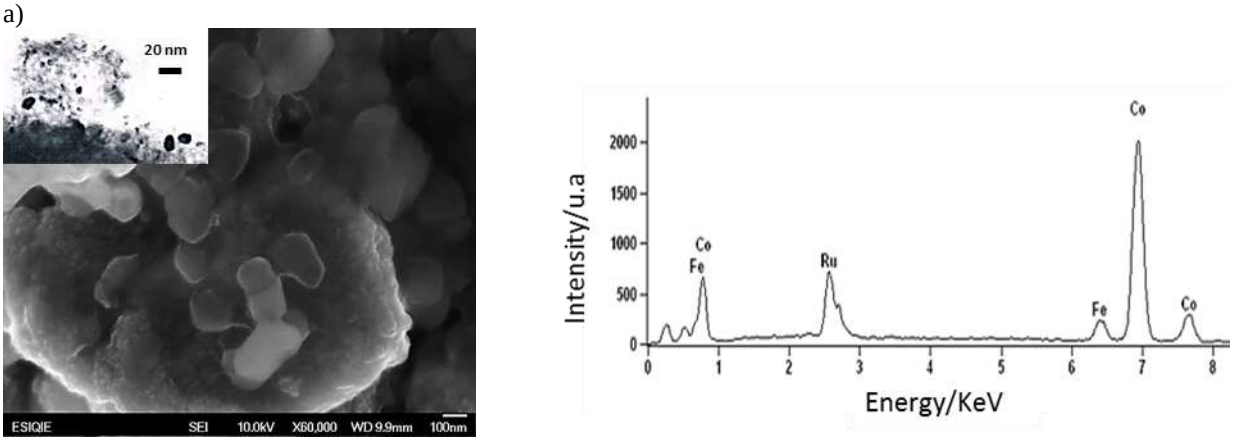

b)

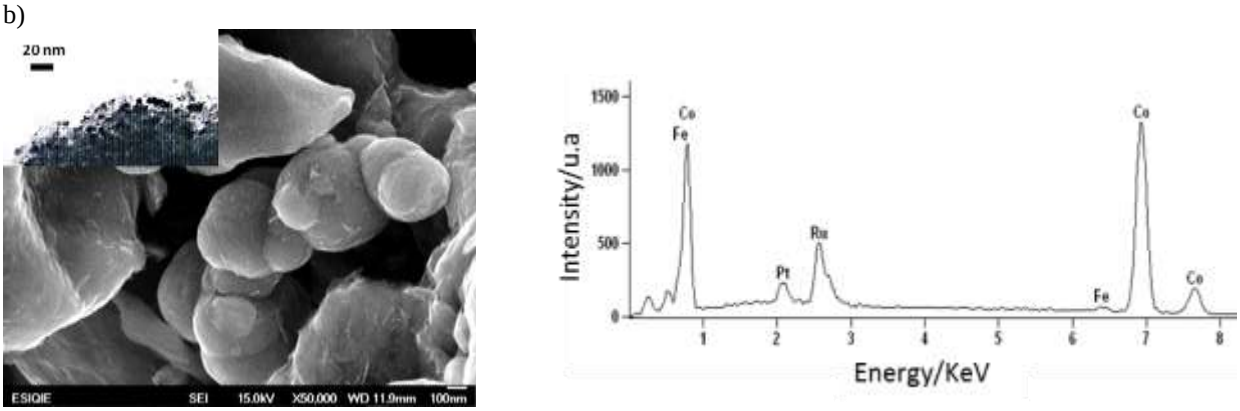

Fig. 2 TEM and SEM images: a) material $Co_{80}Ru_{20}$ and b) material $Co_{80}Ru_{15}Pt_5$ and their respective EDS spectra.

3.3. Electrocatalytic activity toward HER

Polarization curves for the hydrogen evolution reaction (HER) of the synthesized electrocatalytic materials were obtained by potentiodynamic method in a solution 0.5 M H_2SO_4 at a sweep rate of 5 mV s^{-1} and 25 ° C. The polarization was started at open circuit potential and toward negative direction in all cases, Tafel linear polarization measurements were performed to obtain the corresponding electrochemical parameters, fig. 3, such as Tafel slope, exchange current density and transfer coefficient, listed in table 2.

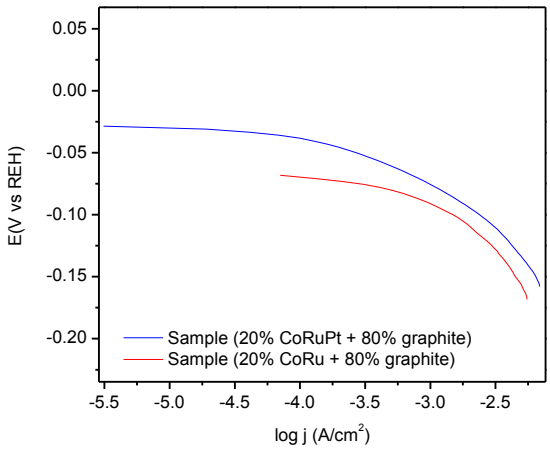

Fig. 3 Linear Tafel polarization curves for the HER of the studied materials, in 0.5 M H_2SO_4 at 5 mV s^{-1}.

Table 2 Kinetic parameters obtained from Tafel curves.

Sample	b_c **(mVdec^{-1})**	α	j_0 **(A cm^{-2})**	η **(mV)** $j = 4\ mA\ cm^{-2}$
Co-Ru	42.8	0.3456	$3.09\ x\ 10^{-4}$	93.1
Co-Ru-Pt	30.4	0.4866	$3.16\ x\ 10^{-4}$	73.1

The absolute value of the Tafel slope, which is an intensive quantity and does not depend on the true surface area of the electrode, is a diagnosis to establish the mechanism and the determining step of the reaction. Slope values close to 40 mV dec^{-1} suggest that the possible mechanism is a classic sequence Volmer-Heyrovsky [15], where the first step is the discharge of the proton by electrosorption:

$$M + H + e^- \leftrightarrow MH_{ads} \qquad Volmer\ reaction \tag{1}$$

The second step in this sequence is the electrochemical desorption:

$$MH_{ads} + H^+ + e^- \leftrightarrow M + H_2 \qquad \text{Heyrovsky reaction} \tag{2}$$

Values close to 29 mV dec^{-1} suggest that the possible mechanism is a Volmer-Tafel sequence [16], where the first step is again discharge electrosorption proton followed by chemical recombination:

$$2MH_{ads} \leftrightarrow 2M + H_2 \qquad Tafel\ reaction \tag{3}$$

Tafel slopes for HER in the studied materials are 30.4 and 42.8 mVdec^{-1} for $Co_{80}Ru_{20}$ and $Co_{80}Ru_{15}Pt_5$, respectively, indicating that the possible reaction mechanism is the classical sequence Volmer -Heyrovsky for

$Co_{80}Ru_{20}$, being the determining step reaction Heyrovsky reaction, whereas for $Co_{80}Ru_{15}Pt_5$ the possible reaction mechanism is the sequence Volmer-Tafel, where the determining step is the reaction of Tafel.

A value of exchange current density is frequently used for the characterization of electrocatalytic activity, so the catalyst $Co_{80}Ru_{15}Pt_5$ showed a better performed because of its value of exchange current density,3.16 x 10^{-4}, although the value of exchange current density for $Co_{80}Ru_{20}$ is close to the last one, 3.04 x 10^{-4}, considering this it was necessary to regard other way to evaluate the performing, it has been reported that values of Tafel slope in the low overpotential region (Tafel region) are as or even more important than a favorable exchange current density value [17]. This is due to the fact that the HER does not occur at a reversible potential, although a certain overpotential is required for the reaction to proceed at a measurable rate. Therefore, in order to compare the electrocatalytic activity of the prepared catalysts, it was fixed a current density and the resulting overpotentials required to reach the given current density value were compared. This has to give an indication of the amount of energy which must be provided to produce a specified amount of hydrogen. Overpotential values for each catalyst, measured at current density of 4 mA cm^{-2} are listed in table 2, $Co_{80}Ru_{15}Pt_5$ required the lowest overpotential to get the current density given, -73.1 mV, on the other hand, $Co_{80}Ru_{20}$ required a larger energy, -93.1 mV. According to the parameters obtained from the studied materials with general composition 80 % graphite + 20% metallic phase, determined by Tafel linear polarization, the material that showed the best performing was $Co_{80}Ru_{15}Pt_5$.

3.4. Electrochemical impedance spectroscopy

To accomplish a better characterization of the interface electrode/electrolyte and the corresponding processes toward the HER in the prepared materials, electrochemical impedance spectroscopy measurements were performed, obtained in a frequency range from 100 kHz to 10 mHz in 0.5 M H_2SO_4 at imposed overpotentials of 0, -10,-25 y -35 mV, other more negative potentials were discarded to avoid possible formation of bubbles over the electrode surface, all measurements were carried at 25 °C.

Fig. 4 presents the complex plane plots (-Z" vs. Z') of both systems, $Co_{80}Ru_{20}$ and $Co_{80}Ru_{20}Pt_5$, obtained at different overpotentials.

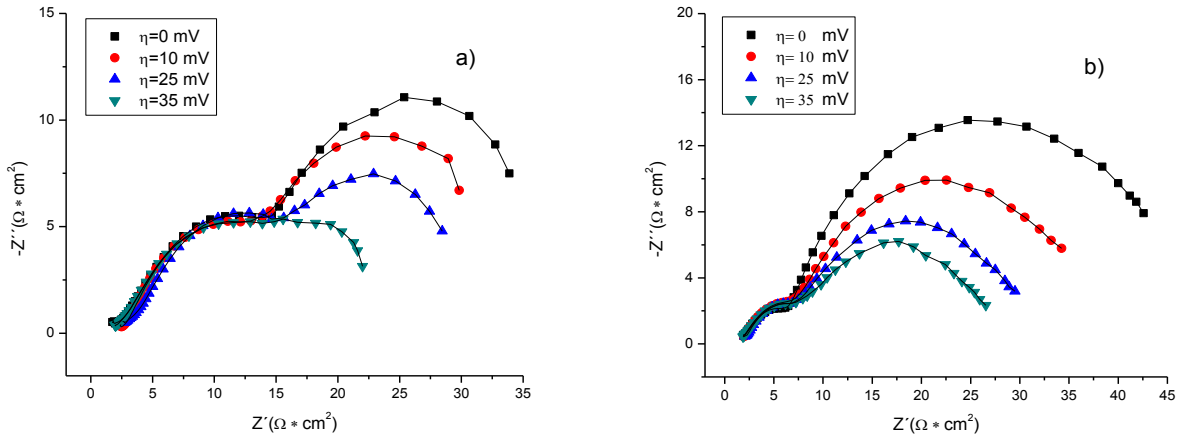

Fig. 4 Nyquist diagrams obtained on a) $Co_{80}Ru_{20}$ and b) $Co_{80}Ru_{20}Pt_5$ in 0.5 M H_2SO_4 at selected overpotentials. The solid lines represent the fitted data using equivalent electrical circuit 2-CPE (→).

It can be observed on Nyquist diagrams the presence of two semicircles: the first at high frequency, where its diameter varies slightly with the overpotential imposed, while the diameter at low frequency decreases considerably as the potential is more negative. From these graphs, there is no a significant difference in the characterization of these materials, inasmuch as both materials are characterized by two time constants. However, qualitatively the detected high frequency semicircle has a diameter smaller for the system $Co_{80}Ru_{15}Pt_5$ than for the system $Co_{80}Ru_{20}$. Preliminarily it could be considered that Pt favors the phenomenon commonly associated with a process electrosorption and/or reduction of protons to the electrode. Generally, the impedance spectra revealed the presence of two time constants, which agrees with the EIS spectra obtained in other electrocatalysts for HER previously studied [18,19].

To describe the electrochemical response and the corresponding processes, experimental EIS data were modeled using NOVA 1.8 software, employing a non-linear fix and an electrical equivalent circuit. Until now three equivalent models have been used to explain the behavior of this kind of electrodes toward HER [20-23]: (i) 1-CPE, (ii) two-CPE and (iii) porous model, the 1-CPE model can produce one or two semicircles on the complex plane plots both of them potential dependent. The second model is the 2-CPE model, introduced by Chen and Lasia [24], this one is commonly used to describe the electrochemical response of two semicircles, the first one, considered potential independent, is associated with the surface porosity and the second one, because of its behavior, is considered potential dependent and can be related to the process of the HER. The third model, introduced by Levie [25], predicts a straight line at 45° at high frequencies, followed by one or two deformed semicircles.

The experimental data for Co- based electrode were simulated using the 2-CPE, fig. 5, consisting of a solution associated resistance, *Rs* in series with two parallel connection of CPE with a resistance, due to the semicircles at high-frequency kept almost constant it was thought to simulate the experimental data using this model. It was tried to use the electrical equivalent model 1-CPE but this model could not be used to describe the experimental *ac* impedance data because the produced circles have to be potential dependent and it did not occur.

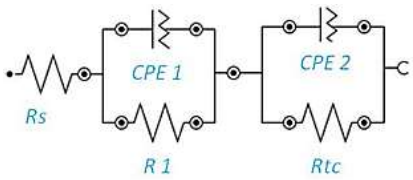

Fig. 5 Electrical equivalent circuit 2-CPE.

From the semicircles at high frequency of Nyquist diagrams it was possible to obtain the parameters *Rs*, A_1, T_1 and ϕ_1, associated with the porosity of the material and therefore they were not affected by the change of overpotential. From the semicircles at low frequency could be found parameters A_2, T_2 *and* ϕ_2, related to the faradic process. Detailed information about the meaning of these parameters is given in Ref. [20-22]. Briefly, the parameter A_2 represents the inverse of the charge transfer resistance R_{TC}:

$$A = \frac{1}{R_{ct}} \tag{4}$$

It was possible determinate parameter T_2 from the impedance given by a CPE, introduced when there is a distribution of the time constants causing a rotation of the semicircle on complex plane:

$$Z_{CPE} = \frac{1}{T(j\omega)^{\phi}} \tag{5}$$

Where ϕ is a constant, taking values from -1 to 1, T is a capacity parameter associated with the double layer capacitance, C_{dl}. When ϕ is equal to 1, T has units of a capacitance, F cm^{-2}. When ϕ is different from 1, T has units expressed in F cm^{-2} s$^{\phi-1}$. To estimate double-layer capacitance, Brug [26] presented a method where faradic process can be expressed by a single equivalent resistance, R_{ct}, as:

$$T = {C_{dl}}^{\phi}\left[{R_s}^{-1} + {R_{ct}}^{-1}\right]^{1-\phi} \quad (6)$$

and finally the capacitances calculated from 6 have units of F cm^{-2}.

Table 3 shows the parameters obtained from EIS analysis. *Rs* is almost constant for each material at different imposed overpotentials, being slightly higher for $Co_{80}Ru_{20}$ system, and this may be due to the variations during the experimentation, such as the distance of the electrodes, the inert atmosphere and/or temperature variation. The behavior is the same for the parameters at high frequency, there is not a noticeable change on CPE_1, ϕ_1 and R_1, taken from high frequency semicircles. On the other hand, parameters taken from low frequency semicircles, it was observed that R_{tc} values for both materials decreased when the applied overpotential was increased, although clearly R_{tc} values for Pt-containing system are lower at more negative overpotentials. It is evident a considerable decrease in value of CPE_2 at values higher of overpotencial to both systems being smaller values for $Co_{80}Ru_{20}Pt_5$.

Table 3 Parameters obtained from electrical circuit equivalent 2-CPE for the studied materials.

System	η (mV)	Rs (Ω cm^2)	CPE_1 (μF cm^{-2})	ϕ_1	R_1 (Ω cm^2)	CPE_2 (μF cm^{-2})	ϕ_2	R_{CT} (Ω cm^2)
$Co_{80}Ru_{20}$	0	2.43	118.43	0.63	15.16	18798.89	0.90	41.73
	10	2.45	81.62	0.56	19.72	18648.30	0.94	37.75
	25	3.02	114.44	0.60	18.18	17234.30	0.94	29.70
	35	2.21	75.71	0.59	19.76	3960.13	0.92	22.78
$Co_{80}Ru_{15}Pt_5$	**0**	1.70	13.27	0.68	4.55	801.49	0.68	42.51
	10	1.76	14.95	0.67	5.51	612.75	0.70	31.00
	25	2.03	14.03	0.72	5.19	404.24	0.71	23.46
	35	1.63	7.10	0.62	4.92	325.15	0.71	18.90

Analyzing Nyquist plots (Z '- Z"), it can observe that for $Co_{80}Ru_{20}$ when a overpotential higher is imposed the semicircle at low frequencies tends to disappear, this can be attributed to rate determining step, as it was discussed above, the reaction mechanism for non-platinum system was the classic sequence Volmer-Heyrovsky at low overpotentials, this behavior is according to H_2 evolution over Ni [27,28], where the Tafel slope must be close to 40 mV dec^{-1}, but after a certain threshold potential, the Tafel slope may increase until it gets a limiting value of 120 mV dec^{-1} [29], so the second stage tends to do not proceed, leading to reduction and/or disappearance of the semicircle. Accordingly, the mechanism for HER in $Co_{80}Ru_{20}$ is Volmer-Heyrovsky.

For $Co_{80}Ru_{20}Pt_5$ is observed the presence of both semicircles at high and low frequencies all imposed overpotentials, establishing the kinetics of the first step is greater than either the kinetics of the reactions desorption or recombination. Considering this, it would be carrying out both reaction adsorption and desorption of protons, both dependent on the potential, as well as the recombination process. From the study of the Tafel slopes was established the reaction mechanism for HER in $Co_{80}Ru_{20}Pt_5$ is Volmer-Tafel. However, EIS study showed that also electrodesorption stage was carried out therefore both stages, after electrosorption, are competing to remove adsorbed species on the surface of the material.

4. Summary and perspectives

XRD analysis showed that there is no the intermetallic formation, analysis of scanning and transmission electron microscopy showed that the synthesized materials formed agglomerates with a size between 1-5 microns, composed by particles smaller than 20 nm, the composition and content of CoRu and CoRuPt were established by means EDS analysis, it could be observed the presence of the characteristic lines of iron, stemming from the grinding media wear, iron modifies the nominal composition, so the weight ratio of Co, Ru and Fe is 73:20:7 for the Co-Ru and for the Co-Ru-Pt the weight ratio of Co, Ru, Pt and Fe is 78:15:5:2. The addition of Pt increases electrocatalytic activity and stability of the material at high potentials. Both materials exhibited good performance toward HER. Tafel slopes for CoRu and CoRuPt were 42.8 and 30.4 mVdec-1, respectively, indicating that the reaction mechanism for this process is Volmer-Heyrovsky for CoRu and Volmer-Tafel for CoRuPt. Tafel analysis showed the material with better electrocatalytic performance is CoRuPt because it is the material with the lowest overpotential value to get at current density of 4 mA cm^{-2}. EIS analysis determined that the kinetics of the material containing Pt was the fastest due to its transfer resistances, extracted from semicircle at low frequency.

Acknowledgements

The authors gratefully acknowledge the financial support provided by Consejo Nacional de Ciencia y Tecnología CONACYT-CNPq 174247, *Instituto de Ciencia y Tecnología del Distrito Federal* ICyTDF 325/2011, Secretaria de Investigación y Posgrado SIP-IPN 20130138 project and Programa Institucional de Formación de Investigadores PIFI-IPN, Sistema Nacional de Investigadores SNI and CONACYT scholarships.

References

[1] A. Miltner, W. Wukoviks, T. Pröll, A. Friedl, Renewable hydrogen production: a thechnical evaluation based on process simulation, www.elsevier.com/locate/jclepro, 2010; 551-562.

[2] J.O'M. Bockris, Energy: The Solar-hydrogen Alternative. Halsted Press, New York, 1975.

[3] J.O'M. Bockris, T.N. Veziroglu, A solar-hydrogen energy system for environmental compatibility. Environ. Conserv., 1985; 12: 105-118.

[4] J.O'M. Bockris, T.N. Veziroglu, D. Smith, Solar Hydrogen Energy: The Power to Save the Earth. Optima, London 1991.

[5] T.N. Veziroglu, F. Barbir, Hydrogen: The wonder fuel. Int. J. Hydrogen Energy, 1992; 17: 391-404.

[6] T.N. Veziroglu, F. Barbir, Solar-hydrogen energy system: the choice of the future. Environ. Conser., 1991; 18: 304-312.

[7] M Ni, MKH Leung, DYC Leung. Energy and exergy analysis of hydrogen production by a proton exchange membrane (PEM) electrolyzer plant. Energy Convers Manage, 2008; 49: 2748-56.

[8] N.K. Labhsetwar, V. Balek, E. Večerníková, P. Bezdička, J. Subrt, T. Mitsuhashi, S. Kagne, S. Rayalu, H. Haneda, J. Colloid Interface Sci., 2006; 30: 232-236.

[9] H. Kita, in Electrochemistyr: The Past Thirty and the Next Thirty Years, H. Bloom and F. Gootman, Eds., Plenum Press, New York, 1977: 117.

[10] K. Lee, J. Zhang, H. Wang, DP Wilinson, Progress in the synthesis of carbon nanotube- and nanofiber-supported Pt electrocatalysts for PEM fuel cell catalysis. J. Appl. Electrochem., 2006; 36: 507-22.

[11] S.A. Grigoriev, M.S. Mamat, K.A. Dzhus, G.S. Walker, P. Millet, Platinum and palladium nano-particles supported by graphitic nano-fibers as catalysts for PEM water electrolysis, Int. J. Hydrogen Energy 2011:36 4143-4147.

[12] P. Paunović, O. Popovski, AT. Dimitrov, D. Slavkov, E. Lefterova, S. Hadži Jordanov, Study of structural and electrochemical characteristics of Co-based hypo-hyper d-electrocatalysts for hydrogen evolution, Electrochim. Acta, 2007; 52: 4640.

[13] C. Barret, Estructure of Metals, McGraw-HillBook Company, Inc. New York, 1957.

[14] G.K. Williamson, W.H. Hall, X-Ray Line Broadening From Filed Aluminium and Wolfram, Acta Metallurgica, 1953; 1: 22.

[15] E. Fachinotti, E. Guerrini, A.C. Tavares, S. Trasatti, Electrocatalysis of H2 evolution by thermally prepared ruthenium oxide, J. Electroanal. Chem., 2007; 600: 103.

[16] J. Chenga, H. Zhanga, H. Ma, H. Zhonga, Y. Zoua, Study of carbon-supported IrO2 and RuO2 for use in the hydrogen evolution reaction in a solid polymer electrolyte electrolyzer, Electrochim. Acta 2010; 55: 1855-1861.

[17] R. Šimpraga, G. Tremiliosi-Filho, S.Y. Qian, B. E. Conway, In situ determination of the "real area factor" in H_2 evolution electrocatalysis at porous Ni-Fe composite electrodes, J. Electroanal. Chem., 1997; 424: 141-151.

[18] E. Ndzebet, O. Savadogo, Study of the hydrogen evolution reaction in a basic-medium on palladium highly dispersed in graphite-electrodes electro-activated with SiW12O404- (STA), Int. J. Hydrogen Energy, 1995; 20: 635-640.

[19] E. Navarro-Flores, Z. Chong, S. Omanovic, Characterization of Ni, NiMo, NiW and NiFe electroactive coatings as electrocatalysts for hydrogen evolution in an acidic medium, J. Mol. Catal. A: Chem., 2005; 226: 179-197.

[20] A. Lasia, Applications of the electrochemical impedance spectroscopy to hydrogen adsorption, Evolution and absorption into metals, In: B. E. Conway and R.E. White, editors Modern Aspects of Electrochemistry, New York: Kluwer/Plenum, 2002; 35: 1-49.

[21] A. Lasia, Electrochemical Impedance Spectroscopy and Its Applications, In: B. E. Conway, J. Bockris and R.E. White, editors Modern Aspects of Electrochemistry, New York: Kluwer/Plenum, 1999, Vol. 32, p. 143-248.

[22] A. Lasia, L. Birry, Studies of the hydrogen evolution reaction on Raney nickel–molybdenum electrodes, J. Appl. Electrochem. 2004; 34: 735-749.

[23] B. Łosiewicz, A. Budniok , E. Rówiński , E. Łągiewka, A. Lasia , The structure, morphology and electrochemical impedance study of the hydrogen evolution reaction on the modified nickel electrodes, Int. J. Hydrogen Energy, 2004; 29: 145-157.

[24] L. Chen, A. Lasia, Study of the Kinetics of Hydrogen Evolution Reaction on Nickel-Zinc Powder Electrodes, J. Electrochem. Soc., 1992; 139: 3214.

[25] R. De Levie, in P. Delahay and C.W. Tobias (eds.), Advances in Electrochemistry and Electrochemical Engineering, Wiley, 1967; 6: 239.

[26] G.J. Brug, A.L.G. Van Den Eeden, M. Sluyters-Rehbach, J.H. Sluyters, The Analysis of Electrode Impedances Complicated by the Presence of a Constant Phase Element, J. Electroanal. Chem., 1984; 176: 275-295.

[27] J.O'M. Bockris, A.K.N. Reddy, Modern Electrochemistry, Plenum, 1970; 2: 1248.

[28] A.J. Appleby, H. Kita, M. Chemla, G. Bronoel, in: A.J. Bard (Ed.), Encyclopedia of Electrochemistry of the Elements, New York, 1982; 9: 383.

[29] J.G. Highfield, E. Claude, K. Oguro, Electrocatalytic synergism in Ni/Mo cathodes for hydrogen evolution in acid medium: a new model, Electrochim. Acta, 1999; 44: 2805-2814.